DESIGN OF COGNITIVE RECEIVER RF FRONT-END CONTROL

Eyosias Yoseph Imana[1], Jeffery H. Reed[2]
(Virginia Polytechnic Institute and State University, Wireless@VT,
Bradley Electrical and Computer Engineering Department,
Blacksburg, Virginia, USA
[1]eyoseph@vt.edu, [2]reedjh@vt.edu).

ABSTRACT

This paper proposes the use of cognitive engine to control the sampling frequency and the local oscillator frequency in a flexible receiver RF front-end. The designed cognitive engine has self-awareness, intelligence and exploitation capabilities. A realistic spectrum occupancy model is developed and used to establish the metrics that are used to evaluate the performances of the cognitive engine. The designed cognitive engine is analyzed theoretically and using simulations. The results of the analysis show that cognitive control can be used to relax the selectivity specifications of receiver RF front-ends.

1. INTRODUCTION

A Software radio (SR) implements most of its functionalities using software running on a generic hardware [1]. Because it is simpler to design, implement and maintain, SR is supposedly cheaper compared to a hardware extensive radio. Furthermore, SR allows radio devices to be used in a manner similar to that of personal computers where the user buys generalized hardware and installs the appropriate software to obtain the operation desired. Such scale of flexibility inspires end-user's innovation, which is vital to maintain the growth of the wireless industry in the 21st century.

When a SR is capable to autonomously select its parameters, it is called cognitive radio (CR) [2]. A CR uses artificial intelligence (AI) to dynamically control its parameters. Currently, CR is primarily being applied in dynamic spectrum access (DSA) based wireless communication systems. The DSA technology allows a secondary user to use a licensed band of the spectrum when it is not being used by its primary user. A DSA CR senses the spectrum and uses AI algorithms to identify the most optimal frequency band to operate in.

One of the challenges facing the wireless industry is that the market's demand for the spectrum is not matched by its availability [3]. This is despite the dramatic improvement in the spectral efficiency of the wireless technology during the past decade. Accordingly, CR is likely to be an integral part of the industry because it allows more efficient use of the spectrum.

In other words, SR and CR technologies have benefits that the wireless industry cannot afford to lose. Nevertheless, SR and CR are not widely adopted because of the difficulties involved in the design their RF front-ends. Any communication radio, including SR and CR, has to incorporate RF front-end between the antenna and the digital signal processing (DSP) section of the radio. However, the RF front-end cannot be very flexible because it is implemented using analog circuitry. To be flexible without sacrificing its key performance measures such as selectivity and dynamic range, the RF front-end typically has to be physically large and complex. This is one of the main reasons why SR and CR have not been favored to be implemented in mobile handsets.

A good illustration for the tradeoff between flexibility and size of RF front-ends is the pre-selector filter in multi-band radios. Small-form-factor tunable RF filters have about 20% 10 dB bandwidth [4], [5], [6], [7] while fixed filters can easily achieve less than 5% 10 dB bandwidth [8]. To maintain its selectivity, a multi-band radio should contain multiple fixed filters which are tuned to different frequency bands. This approach becomes impractical as the number of supported frequency bands increases and the device expands in size. On the other hand, if tunable filters are used, the radio will have manageable size at the expense of degraded selectivity performance.

The filters in receiver RF front-ends are desired to be selective so that the subsequent non-linear elements will be exposed only to a limited amount of undesired signals. Some elements of the RF front-end such as the mixer and the analog-to-digital convertor (ADC) are inherently non-linear; that is, their non-linearity is desired for the normal operation of the radio. Signals which are located at different frequencies at the input of an inherently non-linear element may map to overlapping frequencies at the output. The set of frequencies at the input, which map to the same frequency at the output, are referred as *images*. When a signal passes through a mixer and an ADC, the desired signal is potentially corrupted by the undesired signals which are located at the image frequencies. The other type of RF non-linearity is the undesired non-linearity. This non-

linearity is not vital to the operation of the radio and distorts the signal by creating effects such as intermodulation and crossmodulation distortions. Undesired non-linearity is not the focus of this paper.

The traditional approach to reduce distortion caused by image signals is the inclusion of adequately selective image rejection filters and anti-aliasing filters before the mixer and the sampler, respectively. Adequate image rejection is rarely obtained from tunable pre-selector filters because of their poor selectivity. The direct conversion receiver architecture, supported by IQ imbalance correction within the DSP section of the radio, can be used to effectively remove interference from image signals. If single radio path based architecture is used instead, complexity can be reduced at the expense of image rejection performance of the radio. The high power consumption [9] and large foot print area of highly selective baseband filters also give an incentive to use poorly selective anti-aliasing filters. On the other hand, the spectrum is expected to be more energetic and unpredictable as its demand increases in the future. Hence, the average power per Hz of the radio spectrum is expected to rise.

This paper proposes the use of cognitive RF front-end control to relax the selectivity specification of flexible receiver RF front-ends. Accordingly, the proposed technique can allow poorly selective radios to remain operational in dense spectrum scenarios. Specifically, a cognitive control is applied to dynamically adjust the local oscillator frequency at the down-conversion mixer and the sampling frequency at the ADC to minimize the distortion caused by undesired signals.

The next section introduces the idea of cognitive RF front-end control. Section 3 presents stochastic spectrum occupancy model which is used to develop the performance metrics of the CE that is designed in this paper. Section 4 details the design of the CE and Section 5 describes a simulation-based experiment that was conducted for this research. Finally, section 6 concludes the paper by summarizing its contributions.

2. DESCRIPTION OF A COGNTIVE RF FRONT-END

This section presents the idea of cognitive RF front-end control in a generalized manner. The section also lists the various technologies which inspire the use of cognitive control in RF front-ends.

2.1 Definition and features

A cognitive RF front-end uses AI contained in a cognitive engine (CE) to control the parameters of a flexible RF front-end. The control algorithms adjust the parameters of the RF front-end in accordance to changes in the spectrum and/or changes in the characteristics of the signal of interest.

For example, this paper presents a CE which controls the local oscillator's (LO) frequency and the sampling frequency in receiver RF front-ends. The CE first probes the associated spectrum sensing engine (SSE) to obtain the current state of the spectrum. Then, the CE employs AI algorithms to determine the optimal combination of the LO frequency and sampling frequency which minimizes the total undesired power folding into the frequency band of the desired signal. In such a manner, the CE enables the radio to be adaptive to the RF spectrum on-the-fly.

In general, a cognitive RF front-end should contain three basic units. These are a flexible RF front-end, a spectrum sensing engine (SSE) and a cognitive engine (CE) as shown in Figure 1.

The RF front-end may contain a sensing path in parallel to the main radio path. The sensing and the main path can also be implemented to share the same circuitry in a time-multiplexed manner. The parameters of the sensing path are controlled by the SSE while the parameters of the main path are controlled by the CE.

The SSE meters the state of the spectrum using the measurement carried out through the sensing path. After the CE collects spectrum information from the SSE, it runs its algorithms to determine if the settings of the RF front-end should be altered. If an action has to be taken, the CE initiates command signals to cause the RF front-end to change its current settings. The CE may also probe the RF front-end to obtain awareness of the current state.

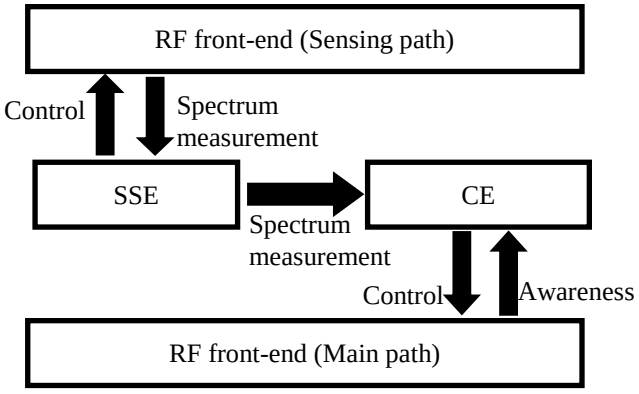

Figure 1. Basic architecture of cognitive RF front-end

A cognitive RF front-end should possess the following features;

- *Sensing*: the cognitive RF front-end contains a sensing engine to reliably measure the state of the spectrum containing the desired signal.
- *Self-awareness*: the CE should be aware of the characteristics of the RF front-end under all the possible settings. This can be done by storing mathematical models describing the RF front-end within the CE or by creating a capability for the CE to probe the RF front-end and measure its characteristics autonomously.

- *Intelligence*: the CE contains algorithms which are designed to optimize parameters of the RF front-end with respect to a pre-defined objective.
- *Exploitation*: A CE should archive the profiles of previous cases and the corresponding solutions proposed by the intelligent algorithms for future reference. If a case whose profile is sufficiently similar to an archived case occurs at later time, the CE can use the associated solution to reconfigure the RF front-end.

Thus, the design of a cognitive RF front-end involves developing a control scheme which implements the aforementioned four features. Section 4 discusses the design of the self-awareness, intelligence and exploitation aspects of a CE which controls the LO frequency and the sampling frequency of a receiver RF front-end. Due to space limitations, this paper will focus only on the design of the CE. The design of the SSE will be detailed in papers which are planned to be released from this research in the near future.

2.2 Enabling technologies

Cognitive control of an RF front-end is practical only if the RF front-end is flexible and can be reconfigured using digital commands. Hence, the enabling technologies of a cognitive RF front-end are those technologies which are improving or are promising to improve the flexibility and controllability of the RF front end.

One enabling technology of cognitive RF front-end is the RF CMOS technology. RF CMOS is favorable to implement reconfigurable RF front-ends because it allows integrating digital and RF circuits on a single chip. Up until the 1990s, CMOS was not ready for RF applications because of its low cut-off frequency [10]. In addition, the simulation models for CMOS were not optimized for RF frequency ranges.

Process technologies have now advanced enough to allow the fabrication of deep sub-micron MOS transistors, which have cut-off frequency in excess of 100 GHz [10]. Research efforts during the past decade, which were aiming to understand the properties RF CMOS, have also contributed to elevate the technology to the level of maturity it has now attained. This is evident by the advent of highly reconfigurable RF CMOS based radio frequency integrated circuits (RFIC) during the past five years [11], [12], [13], [14].

For example, IMEC's [11] RFIC is implemented on 130 nm CMOS technology. This RFIC contains a digital-to-analog convertor (DAC) and an ADC integrated on chip. It operates from 100 MHz to 6 GHz and uses a combination of tunable voltage controllable oscillator (VCO) and divide-and-multiply circuits to implement the LO. Other RF parameters such as bandwidth of baseband filters, gains of amplifiers, bias currents and etc. are all controllable through digital ports provided on the RFIC.

Various research efforts are also underway to further increase the flexibility of RF front-ends. In [15] and [16], IMEC researchers present various techniques that can be used to implement highly flexible baseband radio circuits. The defense advances research projects agency (DARPA) has also recently announced a call for proposal on implementation of RF circuits following the architecture analogous to that of field programmable gate arrays (FPGA) [17].

In conclusion, the level of flexibility of RF front-ends has been increasing and is expected to continue increasing in the future. This encourages the incorporation of AI algorithms to autonomously control the parameters of the RF front-end. This paper shows that such types of control algorithms can be leveraged to relax the selectivity specifications of an RF front-end.

3. MODEL OF SPECTRUM OCCUPANCY

The section describes a stochastic model of spectrum occupancy which is used to analyze the performance of the CE whose design is presented in this paper. The model begins by dividing the spectrum into equal-bandwidth sub-bands. The time durations of spectrum occupancy and vacancy can be modeled by exponential distribution [18]. More specifically, the total duration of the time a sub-band stays occupied by a single detectable signal (a signal above the noise floor), t_{on}, is modeled by exponential distribution which can be expressed as,

$$f_{t_{on}}(t;\lambda_{on}) = \begin{cases} \lambda_{ON} e^{-\lambda_{on} t}, & t \geq 0 \\ 0, & t < 0 \end{cases} \quad (1)$$

Similarly, the duration of time a sub-band stays vacant is also modeled by exponential distribution which can be expressed as,

$$f_{t_{off}}(t;\lambda_{off}) = \begin{cases} \lambda_{off} e^{-\lambda_{off} t}, & t \geq 0 \\ 0 \quad , & t < 0 \end{cases} \quad (2)$$

Note that $E[t_{on}] = \lambda_{on}^{-1}$ and $E[t_{off}] = \lambda_{off}^{-1}$ [19]. Accordingly, the probability that a given sub-band is occupied at any given time can be approximated by,

$$p_{oc} \approx \frac{\lambda_{off}}{\lambda_{on}+\lambda_{off}} \quad (3)$$

In this paper, signals are represented using the average power contained within each sub-band. The term $P(i)$ refers the power received in the i^{th} sub-band. The received power in each sub-band is assumed to refer to the large scale fading power which is obtained by averaging out the effects of small signal fading. This representation is defined as the *power spectrum domain* of the signal.

The developed spectrum occupancy model does not target to depict the distribution of the received power assuming that the transmitter and the receiver are at fixed positions. Rather, this model is designed to capture the

distribution of received power in longer time scales. This model is developed considering the change in the relative position of the transmitter and the receiver. The received power within a sub-band changes if the location of the transmitter changes or if another transmitter starts operating in the sub-band. If a sub-band is occupied, the average power of the received signal within the sub-band is a function of the separation distance between the receiver and the transmitter which is using the sub-band at the time. Therefore, the probability distribution of the power of the signal received by a given receiver is directly related to the probability distribution of the possible positions of the transmitters relative to the receiver.

Let, P_{TX} be the transmission power which is also equal to the maximum possible received power. And let P_{min}, represent the minimum-detectable-signal-power of a receiver. In this model, P_{TX} and P_{min} are assumed to be the same for all transmitters and receivers, respectively. Using the log-normal path-loss model [20], it can be shown that the probability distribution of $P(i)$ follows a truncated-Pareto distribution [21] and is given by the relation in (4). The proof of (4) is listed under the Appendix section. By dropping the sub-band index in $P(i)$ for clarity purposes;

$$f_P(P) = \begin{cases} \left(\frac{P_{min}^{2/n}}{1-\left(\frac{P_{min}}{P_{TX}}\right)^{2/n}} \right) \frac{2}{nP^{1+\frac{2}{n}}}, & P_{min} \le P \le P_{TX} \\ 0, & otherwise \end{cases} \quad (4),$$

where n is the path-loss exponent of the propagation environment. The distribution function given in (4) is obtained by assuming that the sub-band is surely occupied. If this assumption is removed, the probability distribution of the received power for any of the sub-bands is given by,

$$\tilde{f}_P(P) = \begin{cases} \left(\frac{P_{min}^{2/n}}{1-\left(\frac{P_{min}}{P_{TX}}\right)^{2/n}} \right) \frac{2p_{oc}}{nP^{1+\frac{2}{n}}}, & P_{min} < P \le P_{TX} \\ 1-p_{oc}, & P_{min} = P \\ 0, & otherwise \end{cases} \quad (5)$$

The spectrum occupancy model can be expanded to consider the log-normal distributed random shadowing in the path-loss model. The log-normal shadowing parameter is purposely left out from this model to simplify forthcoming analysis. This is a reasonable because purpose of the model is not to accurately depict the spectrum occupancy, but to simply be used as a framework to evaluate the performance of the CE that is designed in this paper.

4. DESIGN OF THE COGNTIVE ENGINE

This section describes the design of a CE which controls the local oscillator frequency (f_{LO}) and the sampling rate (f_s) in flexible receiver RF front-ends. The architecture of the RF front-end which is assumed in this design is shown in Figure 2. The model contains a pre-selector filter, a non-linear LNA, a mixer (which is generally complex), baseband filter and ADC in the RF front-end. After the signal is digitized by the ADC, it is fed into the DSP section which is assumed to be sufficiently selective to the sub-band containing the desired signal. The noise produced by the entire RF front-end is lumped into the noise source which is shown at the input of the RF front-end.

The inherent non-linearity of the mixer and the ADC sampler causes signals which are at different frequencies at the input of the RF front-end to be mapped to the same frequency at the output. The objective of the CE is to find the combination of f_s and f_{LO} which minimizes f_s, under the constraint that the undesired signal power at the desired sub-band does not exceed a pre-defined threshold.

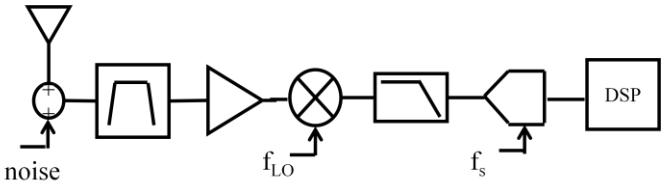

Figure 2. Architecture of RF front-end assumed in this paper

The following sub-sections present how the self-awareness, intelligence and exploitation aspects of the CE are designed in this research.

4.1 Self-awareness

The RF front-end is represented within the CE using parameters of a defined model. This representation creates the self-awareness feature of the CE. This section presents a power spectrum domain based model which is used to characterize the RF front-end within the CE.

Signals which are located at image frequencies at the input of an inherently non-linear element map to the same frequency at the output. If image signals are uncorrelated to each other, the power of the combined signal at the output is the sum of the respective powers of the signals at the input. Assuming that the signals are strictly band-limited within a sub-band (or they are time-unlimited), the assertion that the average power of their combination is equal to the sum of their respective power can be readily proved using the law of conservation of energy.

Figure 2 shows the architecture of the RF front-end that is assumed in this paper. Mixers can be modeled as a cascade of a low-gain amplifier and a balanced switch circuit. Accordingly, the non-linearity and gain of the mixer can be lumped into the non-linearity and gain of the LNA, respectively. For this reason, the RF front-end model developed in this section refers to the mixers as linear switch circuits derived by square wave signal from an

oscillator. The model also neglects the undesired non-linearity of the baseband analog circuit following the mixer.

The RF front-end model developed in this section maps the power spectrum of the signal at the input of the mixer to the power spectrum of the signal at the output of the sampler. The model is independent of the effects of undesired non-linearity in the LNA and the mixer. The model assumes that the pre-selector filter limits the span of the RF spectrum which reaches to the input of the mixer. The non-linearity of the LNA and the mixer expands the frequency span of the spectrum by producing odd-order and even-order intermodulation signals. The odd-order intermodulation signals can be taken as standalone signals in the power spectrum of the signal at the input to the mixer.

Even-order intermodulation signals can appear at baseband by leaking through the mixer, and hence, cannot be directly included in the power spectrum of the signal at the input of the mixer. However, it should be noted that the even-order intermodulation signal at frequency f_1 can also be considered as a standalone signal in the sub-band which contains $f_1 + f_{LO}$ in the power spectrum of the RF signal at the input of a perfectly balanced mixer (with no RF-to-IF leakage). By taking intermodulation signals produced at the LNA (and mixer) as standalone signals in the input spectrum, the RF front-end model is made independent of the effects of undesired non-linearity in the LNA and the mixer. Even though intermodulation products are not expected to follow the distribution in (5), the presentation in this paper assumes that they do to simplify the model.

In summary, only a finite span of spectrum reaches to the input of the mixer. After the complex down-conversion, part of the power spectrum of the signal may map to negative frequencies. The span of the spectrum after the mixer is limited by the baseband filter. The span of the spectrum at the output of the ADC sampler is dependent on the width of the first Nyquisit zone (the sampling frequency).

Let $i: 1 \le i \le M$, $k: -K \le k \le K$, $l: -K \le l \le K$ and $d: -D_{f_s} \le d \le D_{f_s}$ be used to index the sub-bands in the spectrum at the input of the mixer, input of the baseband filter, input of the ADC sampler and output of the ADC sampler, respectively.

Assuming that the local oscillator frequency is always equal to a center frequency of one of the sub-bands of the spectrum at the input of the mixer, the average power of the signal in the k^{th} sub-band at the output of the mixer can be expressed as,

$$P^{MIX}(k; i_{LO}) = P(k + i_{LO}) + \beta P(k - i_{LO}) \quad (6),$$

The term i_{LO} is the index of the sub-band in which the local oscillator frequency is located. Let f_c^j represent the center frequency of the j^{th} sub-band. Then, $f_c^{i_{LO}} = f_{LO}$ and $1 \le i_{LO} \le M$.

Similarly, the average power of the signal in the l^{th} sub-band at the output of the baseband filter is given by,

$$P^{FIL}(l; i_{LO}) = P^{MIX}(l; i_{LO})|H(l)|^2 \quad (7)$$

where $H(l)$ is the frequency response of the filter at f_c^l. If the sampling frequency is also assumed to be equal to center frequency of one of the sub-bands of the spectrum at the input of the ADC, the average power of the signal in the d^{th} sub-band at the output of sampler can be expressed as,

$$P^{ADC}(d; i_{LO}, l_{fs}) = \sum_{m=-\lfloor (K-d)/l_{fs} \rfloor}^{\lfloor (K+d)/l_{fs} \rfloor} Q_m P^{FIL}(d - m l_{fs}) \quad (8)$$

where $f_c^{l_{fs}} = f_s$ and $1 \le l_{fs} \le K$. The $\lfloor \cdot \rfloor$ operator finds the largest and closest integer which is less than a given real number. Note that the summations in (6) and (8) are valid under the assumption that signals in each sub-band are uncorrelated to each other.

For natural sampling with duty-cycle of Δ, Q_m is given by [22],

$$Q_m = sinc^2(m\Delta) \quad (9)$$

The power spectrum of the inputs of the mixer, the filter and the sampler can all be represented in vector format given by,

$$\begin{aligned} \boldsymbol{P} &= [P(1) \quad P(2) \quad \cdots \quad P(M)]^T \\ \boldsymbol{P^{MIX}} &= [P^{MIX}(-K) \;\; P^{MIX}(-K+1) \quad \cdots \quad P^{MIX}(K)]^T \\ \boldsymbol{P^{FIL}} &= [P^{FIL}(-K) \quad P^{FIL}(-K+1) \quad \cdots \quad P^{FIL}(K)]^T \\ \boldsymbol{P^{ADC}} &= \left[P^{ADC}(-D_{f_s}) \quad P^{ADC}(-D_{f_s}+1) \quad \ldots \quad P^{ADC}(D_{f_s})\right]^T \end{aligned} \quad (10)$$

where $D_{f_s} = \lfloor (fs/2)/\Delta f \rfloor$. Therefore, (6), (7) and (8) can be rewritten in matrix form as,

$$\boldsymbol{P^{MIX}}(i_{LO}) = \boldsymbol{A^{MIX}}(i_{LO}) \cdot \boldsymbol{P} \quad (11)$$

$$\boldsymbol{P^{FIL}}(i_{LO}) = \boldsymbol{A^{FIL}} \cdot \boldsymbol{P^{MIX}}(i_{LO}) \quad (12)$$

$$\boldsymbol{P^{ADC}}(l_{fs}, i_{LO}) = \boldsymbol{A^{ADC}}(l_{fs}) \cdot \boldsymbol{P^{FIL}}(i_{LO}) \quad (13)$$

The element at k^{th} raw and i^{th} column in $\boldsymbol{A^{MIX}}(i_{LO})$ is given by,

$$\boldsymbol{A^{MIX}}(k, i; i_{LO}) = \begin{cases} 1, & k = i - i_{LO} \\ \beta, & k = i_{LO} - i \\ 0, & otherwise \end{cases} \quad (14)$$

Similarly,

$$\boldsymbol{A^{FIL}}(l, k) = \begin{cases} H(l), & k = l \\ 0, & otherwise \end{cases} \quad (15)$$

$$\boldsymbol{A^{ADC}}(d, l; l_{fs}) = \begin{cases} Q_m, & d = l - m l_{fs} \\ 0, & otherwise \end{cases} \quad (16)$$

Then,

$$\boldsymbol{A}(l_{fs}, i_{LO}) = \boldsymbol{A^{MIX}}(i_{LO}) \cdot \boldsymbol{A^{FIL}} \cdot \boldsymbol{A^{ADC}}(l_{fs}) \quad (17)$$

Note that the number of rows in $\boldsymbol{A}$ is dependent on the sampling frequency. Finally, from (11)-(13) and (17), it can be easily shown that,

$$\boldsymbol{P^{ADC}}(l_{fs}, i_{LO}) = \boldsymbol{A}(l_{fs}, i_{LO}) \cdot \boldsymbol{P} \quad (18)$$

The relation in (18) gives a simplified power spectrum domain based model for the RF front-end between the mixer and the ADC. The CE becomes *aware* of the RF front-end by acquiring $\boldsymbol{A}$ for every possible i_{LO} and l_{fs} combinations.

4.2 Intelligence and exploitation

The cognitive engine is designed to find the optimal combination of the sampling frequency and LO frequency that minimizes the sampling frequency while maintaining the total power of undesired signals at the input of the DSP unit (Figure 2) below a given threshold (P_{TH}). This section describes how the intelligence and experience-exploitation aspects of the CE are designed.

Let i_d be the index of the sub-band containing the desired signal at the input of the mixer and let $i_d \geq i_{LO}$. If the power spectrum of the input signal is modified by removing the desired signal, the resulting power spectrum is given by $\widetilde{\boldsymbol{P}} = [P(1), \cdots, P(i_d - 1), P_{min}, P(i_d + 1), \cdots, P(M)]^T$.

From (18), the corresponding power spectrum at the output of the ADC sampler is given by,

$$\widetilde{\boldsymbol{P}}^{\boldsymbol{ADC}}(l_{fs}, i_{LO}) = \boldsymbol{A}(l_{fs}, i_{LO}) \cdot \widetilde{\boldsymbol{P}} \quad (19).$$

Note that the frequency of the desired signal maps to the index $d_d = (i_d - i_{LO}) - round\big((i_d - i_{LO})/l_{fs}\big) \cdot l_{fs}$. The operator $round(\cdot)$ finds the nearest integer to a given real number.

Let L_{fs} and I_{LO} be sets of the sub-band indexes of all the possible sampling frequencies and LO frequencies of the RF front-end. And let the combinatory set,

$$S = \{(l_{fs}, i_{LO}) : l_{fs} \in L_{fs}, i_{LO} \in I_{LO}, \widetilde{\boldsymbol{P}}^{\boldsymbol{ADC}}(d_d; l_{fs}, i_{LO}) \geq P_{TH}\} \quad (20)$$

The objective of the CE is to find,

$$(l_{fs}^{opt}, i_{LO}^{opt}) = \begin{cases} \{(l_{fs}, i_{LO}) \in S : l_{fs}^{opt} \leq l_{fs}, \forall\, l_{fs} \in L_{fs}\}, & S \neq \emptyset \\ (l_{fs}^{max}, i_d), & S = \emptyset \end{cases} \quad (21)$$

where l_{fs}^{max} represents the maximum possible sampling frequency. According to (21), the LO frequency can assume any of the possible values as long as the sampling frequency is minimized. Thus, the solution of (21) is not necessarily unique.

The *intelligence* aspect of the CE refers to the capability which allows it to find $(l_{fs}^{opt}, i_{LO}^{opt})$. In this research, this aspect is implemented by a search algorithm which attempts every possible combinations starting from the smallest possible l_{fs} and i_{LO}. Then, the searching process continues by sequentially increasing l_{fs} and i_{LO} until the combination which satisfies the constraint of the set in (20) is obtained. The following sub-section justifies the practicality of implementing this CE as a search algorithm.

From (1) and (2), it can be inferred that there is a finite probability that the occupancy of the image sub-bands of the desired frequency does not change between consecutive spectrum sensing. Therefore, the CE also has an option to use its previous solution if the solution remains satisfying the condition of the set in (20). This option implements the *exploitation* aspect of the CE. The exploitation option reduces the average number of trials the CE takes to obtain a solution. However, there is no guarantee that exploitation produces an optimal solution.

The overall algorithm of the CE designed in this paper is listed below. The CE is assumed to be always aware of $\boldsymbol{A}$ for every possible i_{LO} and l_{fs} combinations.

1. Start
2. Get $(l_{fs}^{opt}, i_{LO}^{opt})$ from previous run
3. Get $\boldsymbol{P}$
4. Get i_d and d_d
5. Compute $\widetilde{\boldsymbol{P}}$
6. Compute $\widetilde{\boldsymbol{P}}^{\boldsymbol{ADC}}(d_d; l_{fs}^{opt}, i_{LO}^{opt})$
7. if $\widetilde{\boldsymbol{P}}^{\boldsymbol{ADC}}(d_d; l_{fs}^{opt}, i_{LO}^{opt}) > P_{TH}$
8. for j from 1 to $|L_{fs}|$
9. for j from 1 to $|I_{LO}|$
10. Compute $\widetilde{\boldsymbol{P}}^{\boldsymbol{ADC}}(d_d; j, i)$
11. if $\widetilde{\boldsymbol{P}}^{\boldsymbol{ADC}}(d_d; j, i) < P_{TH}$
12. $(l_{fs}^{opt}, i_{LO}^{opt}) = (j, i)$
13. return $(l_{fs}^{opt}, i_{LO}^{opt})$
14. end if
15. end for
16. end for
17. $(l_{fs}^{opt}, i_{LO}^{opt}) = (|L_{fs}|, i_d)$
18. return $(l_{fs}^{opt}, i_{LO}^{opt})$
19. else
20. return $(l_{fs}^{opt}, i_{LO}^{opt})$
21. end if

The $|\cdot|$ operator, which is used in line 8 and 9, returns cardinality of a given set. The CE modifies the spectrum reading it receives from the SSE at line 5 by nullifying the power in the desired sub-band. The condition in line 7 checks if a solution obtained in a previous run can be exploited. If the previous solution does not satisfy the condition, the CE searches for a new solution. The algorithm halts and returns at line 13 if a solution which

satisfies the condition in (20) is obtained. If a solution could not be obtained during the search process, the algorithm uses the default solution as shown at line 17. If a previous solution is found to be valid, line 20 is executed to return the previous solution as the current solution.

4.3 Theoretical analysis of the CE

Implementing a CE as a search algorithm potentially makes it slow. This section attempts to address this concern by studying the statistics of the number of steps the CE designed in this paper takes to find a solution. Furthermore, this section also compares the performance of cognitively controlled RF front-end with a perfectly selective RF front-end and a filterless RF front-end.

To simplify the analysis, the filters in the RF front-end are assumed to have an infinite bandwidth. This assumption indicates that the final result of the following analysis will tend to overestimate the actual number of steps the CE takes to find a solution.

Based on this assumption, (8) can be rewritten as,

$$P^{ADC}(d) = \sum_{m=-b}^{b} Q_m\{P(d - ml_{fs} + i_{LO}) + \beta P(d - ml_{fs} - i_{LO})\} \quad (22)$$

where b approaches infinity since the radio is assumed to have no filtering. The probability that $P^{ADC}(d)$ is less than P_{TH} is given by,

$$p_s(P_{TH}) = F_{P^{ADC}}(P_{TH}) \approx \hat{F}_{P^{ADC}}(P_{TH}) \quad (23).$$

where $F_{P^{ADC}}$ represents the cumulative distribution function of P^{ADC}. The subsequent analysis uses $\hat{F}_{P^{ADC}}$ which is an estimate of $F_{P^{ADC}}$ obtained through a Monte Carlo simulation with 1000 instances of $P(d - ml_{fs} - i_{LO})$ and $P(d - ml_{fs} + i_{LO})$ in (22). The summands in (22) were independently generated using the distribution in (4). It should also be noted that for non-impulsive sampling ($\Delta > 0$), $\hat{F}_{P^{ADC}}$ converges as b increases. Hence, a Monte Carlo simulation of (22) with $b > 100$ produces reliable estimate of $F_{P^{ADC}}(P_{TH})$, especially for low P_{TH} values.

If an RF front-end does not contain any filter and the input signal contains only noise, the average power of the signal within any of the sub-bands at the output of the ADC sampler is always greater than P_{min}. This is due to noise-folding to the desired sub-band during the mixing and the sampling processes in the RF front-end. Substituting (9) in (22), and setting $\Delta = 1/2$, the average power of undesired power folded into a desired sub-band at the output of the ADC sampler can be computed as,

$$P'_{min} = P_{min}(1+\beta)\left(1 + \frac{1}{9} + \frac{1}{25} + \cdots\right)\frac{8}{\pi^2} + P_{min}$$

$$P'_{min} = (\beta + 2)P_{min} \quad (24)$$

Accordingly, P'_{min} is the theoretical minimum of the undesired signal power contained in any given sub-band at the output of the ADC sampler.

The set of sub-bands which are images to the desired sub-band at different trials in the search process can loosely be assumed to be different from each other. If the search progresses for long without getting a solution (when P_{TH} is moderately small), the probability that new trials will contain sub-bands which have already been contained in previous trials increases. Hence, assuming that trials in the search process are independent to each other will tend to underestimate the final result of the forthcoming analysis - especially for lower P_{TH} values. For large P_{TH} values, the independent trial assumption compensates the effect of infinite bandwidth assumption. Hence, the final result of the analysis is likely to provide acceptable approximation to the actual number of steps the CE takes to get a solution for large P_{TH} values. These assertions are verified by the results of the simulations presented in the following section.

Under the independent trial assumption, the number of steps the CE takes to obtain a solution is geometrically distributed [19]. Therefore, if the CE is searching for the solution by randomly picking from the possibilities, a solution will be obtained approximately within N_{C} steps with C degree of confidence as shown in (25).

$$N_{\mathrm{C}} \approx \frac{\ln(1 - \mathrm{C})}{\ln\,(1 - p_s(P_{TH}))} \quad (25)$$

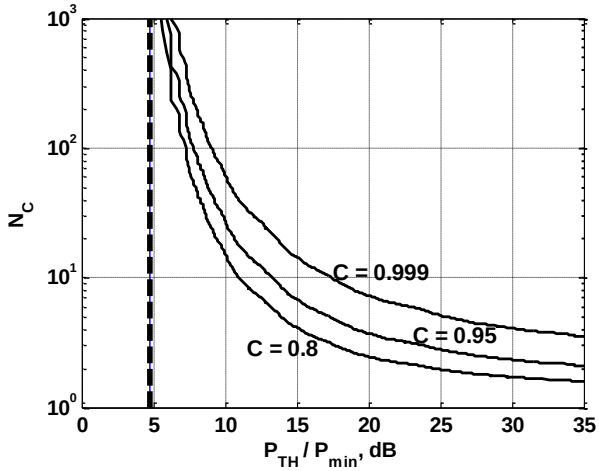

Figure 3. Approximation of the number of steps the CE takes to obtain a solution

Figure 3 presents a plot of N_{c} versus P_{TH} for different degrees of confidence. The plot is obtained by setting $P_{TX} = 30$ dB, $P_{min} = -100$ dBm, $n = 4$, $\beta = 0$ dB, $\Delta = 1/2$, $b = 201$ and $p_{oc} = 0.8$.

The broken line limit at 4.8 dB in Figure 3 represents the minimum possible P_{TH}/P_{min} for filterless RF front-end and is obtained using (24). Figure 3 illustrates that under the spectrum occupancy model developed in Section 3, the CE

takes less than 1000 steps to obtain a solution even for extreme P_{TH} constraints (i.e. P_{TH} within 2 dB of P'_{min}). This means that if each search step takes up to 10,000 clock cycles, then a CE running on a 200 MHz clock can find a solution in less than 50ms almost all the time. Hence, it can be concluded that implementing the CE as a search algorithm does not make it impractically slow.

In addition, the performance of a cognitively controlled RF front-end receiver is compared against conventional RF front-end topologies. Three types of RF front-ends are considered in this comparison. The first one is an ideal radio which is selective enough to pass only the desired signal and sufficiently reject all the other signals except in-band noise in the spectrum. The second type does not have any filters either at RF or at baseband of the RF front-end. The third type is the same as the second type, except that it employs a cognitive control over the RF front-end.

The percentile of the ratio of the undesired power in the desired sub-band at the output of the ADC sampler to P_{min} used as a metric to compare the three types of RF front-ends. If the q^{th} percentile of a random variable x is stated to be z_q, then $\Pr\{x \leq z_q\} = q$. The operator $\Pr\{\cdot\}$ returns the probability of a given random event.

For the first type, since the RF front-end is selective enough, the power of the undesired signal at the sub-band of the desired signal is P_{min} for any q. Hence, the percentile of undesired power for the first type RF front-end is given by,

$$z_q^1 = P_{min} \quad (26).$$

For the second type of RF front-end, the percentile of the undesired power is given by,

$$z_q^2 = \hat{F}_{P^{ADC}}^{-1}(q) \quad (27).$$

For the third type of RF front-end, the percentile of the undesired power can be obtained in terms of the number of CE trials (N) by rearranging (25) and substituting in (27). Accordingly,

$$z_q^3 = \hat{F}_{P^{ADC}}^{-1}(1 + (1-q)^N) \quad (28).$$

Figure 4 compares the percentile of the average undesired powers obtained for the different types of RF front-ends in (26), (27) and (28). The plots are obtained by setting $P_{TX} = 30$ dB, $P_{min} = -100$ dBm, $n = 4$, $\beta = 0$ dB, $\Delta = 1/2$, $b = 201$ and $p_{oc} = 0.8$. The figure shows that the performance bound of cognitively controlled filterless RF front-end (P'_{min}) is within 5 dB of the percentile power of a perfectly selective filter (P_{min}).

The plot in Figure 4 illustrates that applying cognitive control has enabled a filterless, 0 dB image rejection RF front-end to behave similar to a perfectly selective RF front-end. Consequently, it can be concluded that cognitive control can be used to relax the selectivity specifications of the receiver RF front-ends. The benefit of the CE is significant for the low P_{TH}/P_{min} region. For example, a filterless radio achieves a $P_{TH}/P_{min} = 10$ dB performance almost 100 % of the time if the 100 step CE is employed and only about 10% of the time if the CE is not employed. The improvement in the low P_{TH}/P_{min} region is highly desired because the power of the desired signal is typically close to P_{min} as predicted by (4).

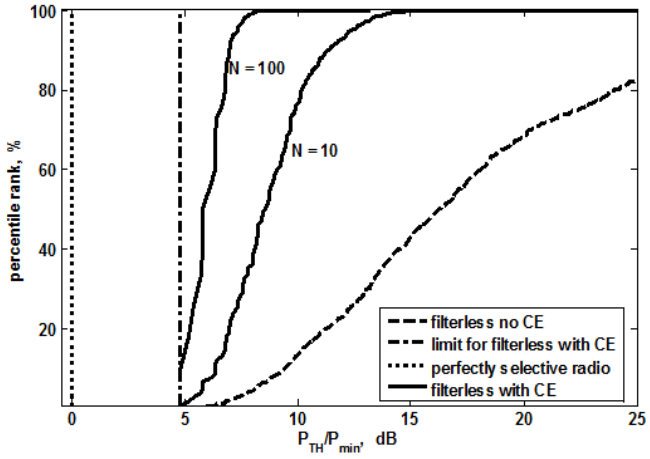

Figure 4. Percentile power for different types of RF front-ends

5. SIMULATION

A power spectrum domain based simulation of a receiver RF front-end was carried out to verify the design of the CE presented in the previous section. The span of the spectrum reaching the inputs of the mixer was set to be limited between 850 MHz to 950 MHz. This span of the spectrum was divided to one thousand 100 kHz wide sub-bands. The image rejection ratio in the mixer was set to be 0 dB. The baseband filter was designed based on 2nd order Butterworth topology and was set to have a cut-off frequency at 10 MHz. The desired frequency was set to be at 900 MHz in the input spectrum. The power level in each sub-band was generated using the distribution in (5), by setting the path-loss exponent of the environment (n) to be equal to 4. The power of the minimum detectable signal was set to be -100 dBm and the transmission power was set to be 30 dBm for all transmitters. In addition, $\lambda_{on} = 1/8$ and $\lambda_{off} = 1/2$ ($p_{oc} \approx 80\%$) were used to govern the change in the level of the received power in each sub-band.

The simulation of the CE runs to find the combination of f_s and f_{LO} which minimizes f_s and ensures that the total undesired power at the desired sub-band at the output of the

Table 1. Simulation results

P_{TH}/P_{min} (dB)	With exploitation		Without exploitation			Theoretical Approximation $N_{0.95}$
	Average N	Average f_s^{opt} (MHz)	Average N	Average f_s^{opt} (MHz)	$N_{0.95}$	
5.5	245	3.4	320	2.8	714	998
6.0	125	1.8	160	1.6	405	374
8.0	55	1.4	160	1.6	235	67
10.0	25	0.6	40	0.5	95	20
15.0	5	0.4	10	0.3	44	6
20.0	1	0.2	1	0.2	3	4
30.0	1	0.2	1	0.2	1	2

ADC is less than P_{TH}. The allowed sampling frequencies range from 200 KHz to 20 MHz, at steps of 200 KHz. The allowed LO frequencies range from 900 MHz to 910 MHz, also at steps of 200 KHz.

The simulation was set to measure two parameters. These are the number of steps the simulated CE takes to obtain a solution and the sampling frequency suggested by the CE (f_s^{opt}) at each run. These parameters were measured by running the CE with and without the exploitation option, but using the same spectrum occupancy data. The simulation was carried out by varying P_{TH} from -94.5 to -70 dBm. The simulation was rerun 100 times and the averages of the measurements obtained from each run were recorded. The results are presented in Table 1. The estimate of the 95% percentiles of the number of steps the CE takes to find a solution were also obtained and compared with the values predicted by the theoretical expression in (25). The results are also shown in Table 1.

The results shown in Table 1 illustrate that the theoretical results obtained in the previous section are reasonably accurate to predict performance of the CE in poorly selective radios. The results from the simulation are within an order of magnitude from the result obtained from the theoretical approximation. The results in Table 1 also show that exploitation has a potential to reduce the average number of steps needed to find the solution by selecting sub-optimal sampling frequencies.

6. CONCLUSION

The recent advances in the flexibility of RF technologies are allowing the incorporation of cognitive control in the design of RF front-ends. This paper proposes the use of cognitive control to relax the selectivity specifications of the RF front-end. This paper shows that poorly selective RF front-ends, which are typical in flexible receivers, can perform in a manner comparable to perfectly selective filters by cognitively controlling the sampling frequency and the LO frequency in the RF front-end.

The design of a cognitive engine (CE) which implements the self-awareness, intelligence and exploitation aspects of a cognitive RF front-end are presented in this paper. This paper proposes the use of a linear power spectrum domain based model to create the awareness of the RF front-end from within the CE. The intelligence and exploitation aspects of the CE were implemented within a reliable but simple brute-force-search like algorithm. In addition, theoretical and simulation based analysis are carried out to approximate the number of trials the designed CE takes to find a solution. The results of the analysis prove that it is feasible to implement the CE as a search algorithm.

This research plans to release other papers on the design of the SSE and on the hardware implementation of the CE and the SSE.

7. APPENDIX

Probability distribution function of received power

According to the free-space path-loss model, the power of the signal received from a transmitter located a distance of r from the receiver is given by,

$$P = \frac{K \cdot P_{TX}}{r^n} \qquad \text{(a. 1)},$$

where K is a constant which is a function of frequency, n is the path-loss exponent and P_{TX} is the transmission power.

The maximum separation distance, r_{max}, corresponds to the minimum power of a detectable signal. Hence, it can be shown that,

$$P = \frac{P_{min}}{\alpha^n} \qquad \text{(a. 2)},$$

where $\alpha = r/r_{max}$. A transmitter can be located anywhere around the receiver except within radius of $r_{min} = \alpha_{min} r_{max}$. Assuming that the received power equals P_{TX} when $r = r_{min}$, it can be shown that,

$$P_{TX} = \frac{P_{min}}{\alpha_{min}^n} \qquad \text{(a. 3)}.$$

The probability that a transmitter is located within radius of r from a receiver which has detected the transmitted signal is given by $(\pi r^2 - \pi r_{min}^2)/(\pi r_{max}^2 - \pi r_{min}^2)$. Therefore, the cumulative distribution function of α can be expressed as,

$$F_\alpha(\alpha) = \begin{cases} 0, & \alpha < \alpha_{min} \\ \frac{\alpha^2 - \alpha_{min}^2}{1-\alpha_{min}^2}, & \alpha_{min} \le \alpha \le 1 \\ 1, & \alpha > 1 \end{cases} \quad \text{(a.4)}.$$

From (a.2) it can be shown that the cumulative distribution function of P is given by $F_P(P) = 1 - F_\alpha\left(\sqrt{P_{min}/P}\right)$. Substituting in (a.4) it can be shown that,

$$F_P(P) = \begin{cases} 0\,, & P < P_{min} \\ \frac{1-\left(\frac{P_{min}}{P}\right)^{2/n}}{1-\left(\frac{P_{min}}{P_{TX}}\right)^{2/n}}\,, & P_{min} \le P \le P_{TX} \\ 1\,, & P > P_{TX} \end{cases} \quad \text{(a.5)}.$$

Finally, the probability density function of P which is obtained by differentiating F_P in (a.5) is given by,

$$f_P(P) = \begin{cases} \left(\frac{P_{min}^{2/n}}{1-\left(\frac{P_{min}}{P_{TX}}\right)^{2/n}}\right)\frac{2}{nP^{1+\frac{2}{n}}}\,, P_{min} \le P \le P_{TX} \\ 0\,, \quad otherwise \end{cases} \quad \text{(a. 6)}$$

8. REFERENCES

[1] J. I. Mitola, "Software radios-survey, critical evaluation and future directions," *IEEE Aerospace and Electronic Systems Magazine*, vol. 8, no. 4, pp. 25-36, 1993.

[2] J. I. Mitola, "Cognitive Radio: An Integrated Agent Architecture for Software Defined Radio," Ph.D. Dissertation, Royal Institute of Technology, Kista, Sweden, 2000.

[3] Federal communications Commission, "Mobile broadband: the benefits of additional spectrum," FCC, Washington, D.C., 2010.

[4] M. Roy and J. Richter, "Tunable ferroelectric filters for software defined tactical radios," in *Proc. 15th IEEE International Symposium on the Applications of Ferroelectrics, pp.348-351, 2006*.

[5] M.-T. Nguyen, W. Yan and E. Horne, "Broadband tunable filters using high Q passive tunable ICs," in *IEEE MTT-S International Microwave Symposium Digest, , pp.951-954, 2008*.

[6] A. Brown and G. Rebeiz, "A varactor-tuned RF filter," *IEEE Transactions on Microwave Theory and Techniques*, vol. 48, no. 7, pp. 1157-1160, 2000.

[7] A. Malczewski, B. Pillans, F. Morris and R. Newstrom, "A family of MEMS tunable filters for advanced RF applications," in *IEEE MTT-S International Microwave Symposium Digest, pp.1-4, 2011*.

[8] A. Coon, "SAW filters and competitive technologies: a comparative review," in *Proc. of IEEE Ultrasonics Symposium, pp.155-160 vol.1, 1991*.

[9] P. Baltus, "Minimum power design of RF Front Ends," Ph.d. Dissertation, Technische University, Eindhoven, 2004.

[10] T. Lee, "From Oxymoron to Mainstream: The Evolution and Future of RF CMOS," in *IEEE International Workshop on Radio-Frequency Integration Technology*, Singapore, 2007.

[11] J. Craninckx, M. Liu, D. Hauspie, V. Giannini, T. Kim, J. Lee, M. Libois, D. Debaillie, C. Soens, M. lngels, A. Baschirotto, J. Van Driessche, L. Van der Perre and P. Vanbekbergen, "A Fully Reconfigurable Software-Defined Radio Transceiver in 0.13µm CMOS," in *IEEE International Solid-State Circuits Conference Digest of Technical Papers, pp.346-607*, 2007.

[12] M. Ingels, C. Soens, J. Craninckx, V. Giannini, T. Kim, B. Debaillie, M. Libois, M. Goffioul and J. Van Driessche, "A CMOS 100 MHz to 6 GHz software defined radio analog front-end with integrated pre-power amplifier," in *Proc. 33rd European Solid State Circuits Conference, pp.436-439*, 2007.

[13] G. Cafaro, T. Gradishar, J. Heck, S. Machan, G. Nagaraj, S. Olson, R. Salvi, B. Stengel and B. Ziemer, "A 100 MHz 2.5 GHz Direct Conversion CMOS Transceiver for SDR Applications," in *Proc. IEEE Radio Frequency Integrated Circuits (RFIC) Symposium, pp.189-192*, 2007.

[14] Lime Microsystems, "LMS6002D configurable broadband transceiver IC," Lime Microsystems, 2011. [Online]. Available: http://www.limemicro.com/lms6002d.php. [Accessed 3 August 2012].

[15] V. Giannini, J. Craninckx, S. D'Amico and A. Baschirotto, "Flexible Baseband Analog Circuits for Software-Defined Radio Front-Ends," *IEEE Journal of Solid-State Circuits*, vol. 42, no. 7, pp. 1501-1512, 2007.

[16] V. Gianni and J. Craninckx, Baseband analog circuits for software defined radio, Dordrecht, The Netherlands: Springer, 2008.

[17] DARPA Microsystems Technology Office, "Board Agency Annoucement, Radio Frequency-Field Programmable Gate Arrays (RF-FPGA) [DARPA-BAA-12-13]," DARPA, 2011.

[18] C. Ghosh, S. Pagadarai, D. Agrawal and A. Wyglinski, "A framework for statistical wireless spectrum occupancy modeling," *IEEE Transactions on Wireless Communications*, ,vol. 9, no. 1, pp. 38-44, 2010.

[19] S. Ross, First Course in Probability, 8th edition, Prentice Hall, 2009.

[20] T. S. Rappaport, Wireless Communications; Principles and Practice, Prentice Hall, 1996.

[21] L. Zaninetti and M. Ferraro, "On the truncated Pareto distribution with applications," *Central European Journal of Physics*, vol. 6, no. 1, pp. 1-6, 2008.

[22] L. I. Couch, Digital and Analog Communication Systems, Prentice Hall, 1992.